Biophysical *Journal*
Computational Tool

Biophysical Society

FEATHER: Automated Analysis of Force Spectroscopy Unbinding and Unfolding Data via a Bayesian Algorithm

Patrick R. Heenan[1,2] and Thomas T. Perkins[1,3,*]
[1]JILA, National Institute of Standards and Technology, [2]Department of Physics, and [3]Department of Molecular, Cellular, and Developmental Biology, University of Colorado, Boulder, Colorado

ABSTRACT Single-molecule force spectroscopy (SMFS) provides a powerful tool to explore the dynamics and energetics of individual proteins, protein-ligand interactions, and nucleic acid structures. In the canonical assay, a force probe is retracted at constant velocity to induce a mechanical unfolding/unbinding event. Next, two energy landscape parameters, the zero-force dissociation rate constant (k_o) and the distance to the transition state ($\Delta x^{\ddagger}$), are deduced by analyzing the most probable rupture force as a function of the loading rate, the rate of change in force. Analyzing the shape of the rupture force distribution reveals additional biophysical information, such as the height of the energy barrier ($\Delta G^{\ddagger}$). Accurately quantifying such distributions requires high-precision characterization of the unfolding events and significantly larger data sets. Yet, identifying events in SMFS data is often done in a manual or semiautomated manner and is obscured by the presence of noise. Here, we introduce, to our knowledge, a new algorithm, FEATHER (force extension analysis using a testable hypothesis for event recognition), to automatically identify the locations of unfolding/unbinding events in SMFS records and thereby deduce the corresponding rupture force and loading rate. FEATHER requires no knowledge of the system under study, does not bias data interpretation toward the dominant behavior of the data, and has two easy-to-interpret, user-defined parameters. Moreover, it is a linear algorithm, so it scales well for large data sets. When analyzing a data set from a polyprotein containing both mechanically labile and robust domains, FEATHER featured a 30-fold improvement in event location precision, an eightfold improvement in a measure of the accuracy of the loading rate and rupture force distributions, and a threefold reduction of false positives in comparison to two representative reference algorithms. We anticipate FEATHER being leveraged in more complex analysis schemes, such as the segmentation of complex force-extension curves for fitting to worm-like chain models and extended in future work to data sets containing both unfolding and refolding transitions.

INTRODUCTION

Over the last ~25 years, single-molecule force spectroscopy (SMFS) has emerged as a powerful tool to quantify diverse biological systems, including the strength of protein-ligand bonds (1,2) and the unfolding and refolding of individual protein domains (3,4). In one widely used assay, an atomic force microscopy (AFM) cantilever or an optically trapped bead is attached to the biological system under study and retracted at a constant velocity (Fig. 1 *A*). Force is deduced as the displacement of the force probe away from its equilibrium position. Abrupt drops in force at the rupture force arise from unfolding/unbinding events (Fig. 1 *B*). Because these events are thermally activated, there is not a unique rupture force but rather a distribution (Fig. 1 *C*). The Bell-Evans model rapidly emerged as a way to characterize a one-dimensional projection of the underlying free-energy landscape along the stretching axis (2,5,6). In this analysis, a fit to the most probable rupture force as a function of loading rate yields the following two parameters: the zero-force dissociation rate constant (k_o) and the distance to the transition state ($\Delta x^{\ddagger}$) (Fig. 1 *D*). More advanced models that analyze the shape of the F_R distribution provide additional information on the free-energy landscape such as the height of the energy barrier ($\Delta G^{\ddagger}$) (7) but require higher precision event detection and larger numbers of events. Yet, event detection is obscured because of the presence of Brownian motion and instrumental noise and is often done manually or in a semiautomated manner, including in recent work from our lab (8). Thus, accurately quantifying hundreds

Submitted April 13, 2018, and accepted for publication July 20, 2018.
*Correspondence: tperkins@jila.colorado.edu
Editor: Keir Neuman.
https://doi.org/10.1016/j.bpj.2018.07.031

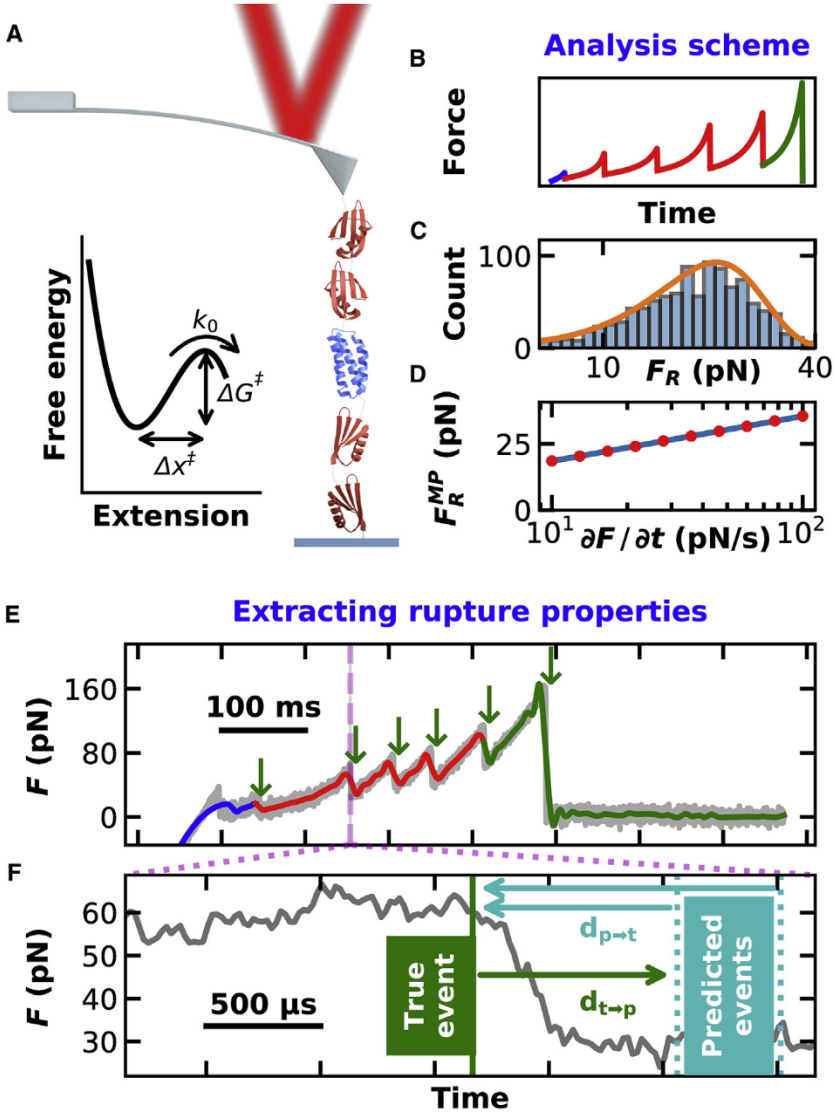

FIGURE 1 For a Figure360 author presentation of Fig. 1, see the figure legend at https://doi.org/10.1016/j.bpj.2018.07.031. Figure360▷

An overview of force spectroscopy analysis is shown. (*A*) A cartoon illustrating an AFM cantilever unfolding a polyprotein containing four mechanically robust domains (NuG2, *red*) and one mechanically labile one (α_3D, *blue*) is shown. (*Inset*) A sketch of a one-dimensional free-energy landscape and the following associated parameters is shown: k_o, the zero-force dissociation rate constant; $\Delta x^\ddagger$, the distance to the transition state; and $\Delta G^\ddagger$, the height of the energy barrier. (*B–D*) A typical analysis scheme for a polyprotein unfolding assay illustrated with a computationally generated data set based on a model by Dudko et al. (7) is shown. (*B*) A force-versus-time curve for the unfolding of the polyprotein with segments color coded based on the domain before unfolding is shown. (*C*) A distribution of rupture forces (F_R) for the α_3D domain fitted to the Dudko model is shown. (*D*) The most probable rupture force (F_R^{MP}) versus the log of the loading rate ($\partial F/\partial t$) fitted with a line per the Bell-Evans model (2,5,6) is shown. (*E*) An experimental force-versus-time curve of the polyprotein shown in (*A*), with unfolding events marked by green arrows, is shown. Color-coded data were smoothed to 500 Hz with higher-bandwidth data (50 kHz) plotted in gray. (*F*) A high-time-resolution plot of a single rupture event was used to define the metrics for comparing automated algorithms: a true event is manually defined by an expert user as detailed in the Supporting Materials and Methods; $d_{t\to p}$ is the distance from a true event to the closest predicted event; and $d_{p\to t}$ is the distance from an algorithmically predicted event to the closest true event. Predicted events are illustrative, not actual.

to thousands of rupture events in an automated, reliable, and reproducible way is critical for gaining insight into the diverse biomolecular systems studied by SMFS.

To address this need, multiple groups have developed algorithms to detect rupture events in AFM data and other SMFS modalities. For example, such techniques have applied worm-like chain models to compute contour lengths at each extension (9,10), used thresholding based on signal or noise characteristics (11,12), and classified traces based on transformations of the data into frequency or derivative spaces by spatially localized Fourier series or wavelets (13–15). These methods provide increased automation, but their use is limited by their lack of generalization. Ongoing efforts and interest in automated analysis continues (e.g., recent work integrated several steps in SMFS analysis of unfolding data into a single package (16)). Contour-length alignment algorithms bias results toward dominant features and necessarily require a model. Thresholding or transformation algorithms typically require many parameters. For example, previous techniques have six (14,15) and even up to 14 or 17 parameters (16,17). Large numbers of parameters help tune an algorithm to a particular data set, but they also increase the search space for parameter optimization and may be difficult to apply to data sets containing unfolding events occurring over a broad range of forces.

Here, we present, to our knowledge, a new algorithm for detecting unfolding/unbinding events and apply it to SMFS data sets representative of a variety of typical experimental conditions. The algorithm, named FEATHER (force extension analysis using a testable hypothesis for event recognition), requires no special knowledge of a specific system's polymer properties, detects both rare and dominant data behavior, and outperforms recently published algorithms over a wide range of pulling velocities, two common systems of interest (polyproteins and DNA), and a computationally generated data set. FEATHER is a Bayesian

algorithm because it computes the probability of each point in the retraction curve given a model automatically calculated from the event-free approach curve. Because FEATHER's improved performance requires just two easy-to-interpret parameters, a smoothing factor and a significance threshold, we anticipate FEATHER being leveraged to improve the throughput, quality, and reproducibility in SMFS analysis schemes.

Materials and Methods

FEATHER is written in Python 2.7, with interfaces written for MATLAB (The MathWorks, Natick, MA) and Igor Pro. The source code, working examples, and accompanying documentation is freely available (https://doi.org/10.5281/zenodo.1319742). Importantly, for analyzing large data sets, FEATHER's execution time scaled linearly with the number of data points and offered an order of magnitude improvement in runtime relative to the faster of the two algorithms used for comparison (Fig. S1). The basis for the statistical analysis used by FEATHER and all performance metrics are presented in the Supporting Materials and Methods. All timing and tuning results were obtained using a desktop personal computer with 32 GB of RAM, an Advanced Micro Devices Ryzen 5 1500× Quad-Core CPU, and a 500-GB hard drive. To test FEATHER, we used the following two data sets: 1) 152 force-extension curves of a previously described polyprotein that contains one mechanically labile target protein (α_3D) with a measured change in contour length (ΔL_0) of 23 nm upon rupture (8) positioned between four mechanically robust marker domains of NuG2 ($\Delta L_0 = 18$ nm per NuG2 monomer (18)) (Fig. 1 *A*; Table S1), and 2) 600 force-extension curves of DNA deposited at purposely high surface coverage to promote multiple tip-DNA attachments and therefore multiple rupture events per force-extension curve (Fig. S2; Tables S2 and S3). As described in detail in the Supporting Materials and Methods, both data sets contained curves acquired over a range of retraction velocities (v). Finally, FEATHER's performance was tested using a simulated data set containing force-extension curves that were purposely challenging to analyze, as described in the Supporting Materials and Methods.

Results and Discussion

Description of FEATHER

In SMFS, unfolding events occur when the force applied to a molecule exhibits an abrupt drop in a force-versus-time curve as the molecular configuration passes over an energy barrier (Fig. 1 *E*, *green arrows*). To determine the location of such events, FEATHER first fits a smoothing spline to the raw data (Fig. 2 *A*) with nodes in the spline spaced at a user-defined fractional spacing (τ) of the full record length, so the temporal averaging time (5–50 ms) depends on v given a fixed data acquisition rate, as is typical in such assays. Although the model defined by the spline has a continuous first derivative, unfolding events exhibit a discontinuity in the first derivative. Thus, unfolding events could be located by computing when the data were inconsistent with the model. To efficiently detect short-lived events, we recommend users choose the largest τ that preserves such events in the smoothed data (Fig. S3).

To compute the statistical significance of an unfolding event at time t, we constructed a no-event hypothesis based on the noise characteristics of the data relative to a reference curve lacking any events. For AFM data, the approach curve taken with the same individual cantilever served as an excellent reference. Briefly, the process of computing the significance (P) of an event started by subtracting the smoothing

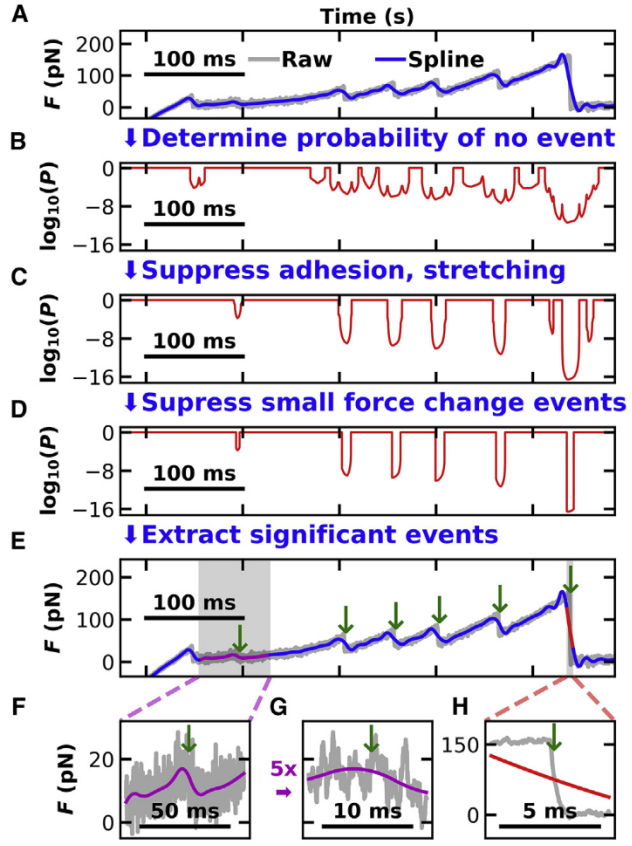

FIGURE 2 FEATHER's analysis scheme. (*A*) A high-bandwidth force-versus-time record of polyprotein unfolding (*gray*) with FEATHER's spline fit overlaid in blue, where $\tau = 15$ ms, is shown. (*B*) The probability (P) of a nonevent was obtained by applying Chebyshev's inequality to the record in (*A*). Unfolding events occur when this probability is near 0. (*C*) The probability from (*B*) transformed to de-emphasize regions near the surface and regions with positive force derivatives is shown. (*D*) The probability from (*C*) was further modified to suppress regions where the force change was negligible, as determined from a reference curve with no events (e.g., the approach). (*E–H*) Force-versus-time curves and magnified regions highlight event determination, indicated by green arrows using a significance threshold of $P_{\text{thresh}} = 0.001$, are shown.

spline from the high-bandwidth data to yield a force residual with a zero-centered mean and variance about that mean (which contained mostly the thermal noise of the system within a fractional size of the record defined by τ). The magnitude of this residual variance as a function of time is compared to the approach curve that contained no unfolding/refolding events. Alternatively stated, we determined how the variance of the force variance changes in time because this metric was found to be insensitive to local variation in curvature of the data but highly sensitive to unfolding events (Fig. S4 *F*). Deviation from this mean magnitude of residual noise was transformed into a probability using Chebyshev's inequality (Eq. S1), which importantly does not assume any form of the noise distribution (19). We note that FEATHER requires that the noise distribution of the force residuals have zero mean and median but otherwise does not impose constraints on the distribution.

Empirically, we observed the statistical significance of an event was enhanced by combining the no-event probability for the force in combination with the integral force, force derivative, and force differential, all conceptually based on the same implementation of Chebyshev's inequality, as shown in Eq. S2. For instance, the probability from Fig. 2 *B* was transformed to de-emphasize stretching of the construct in which the force derivative is positive or negligible, and surface adhesion was ignored by including only events that started after the tip was retracted off of the surface (Fig. 2 *C*). We next suppressed events associated with small force changes consistent with the force noise in the reference (or approach) curve (Fig. 2 *D*) as described in the Supporting Materials and Methods (Fig. S4; see pseudocode listed in Table S4). Events were identified from the probability shown in Fig. 2 *D* based on a user-defined threshold (e.g., $P_{\text{event}} = 0.001$) (Fig. 2 *E*). Importantly, FEATHER correctly identified rupture events even though the rupture force varied by an order of magnitude within the same record (Fig. 2, *F–H*). Moreover, this high-fidelity event detection was insensitive to an ~10-fold variation in τ and the thresholding parameter (P_{event}), in contrast to other event detection algorithms (see Supporting Materials and Methods; Figs. S3 and S5).

Evaluating FEATHER's performance

We evaluated the performance of FEATHER to accurately and precisely analyze the unfolding of our polyprotein, which exhibited both low- and high-force ruptures. Specifically, we compared how well FEATHER did relative to manually annotated data from an expert user and two automated analysis routines, the recently published OpenFovea (12) and the wavelet scheme "find_peaks_cwt" method from Scientific Python (20). These algorithms were chosen to provide a representative sample of the viable techniques used in AFM data analysis because they respectively utilized thresholding and wavelet transformations, which are two broad classes of event-detection techniques. In addition, neither of these reference algorithms requires specialized knowledge of the polymer under study like the worm-like chain model commonly used in contour-length alignment algorithms. The following three primary metrics were used: the relative location error, the loading rate, and the rupture force (Fig. 3). We note that each algorithm outputs a list of predicted event locations; the loading rate and rupture force were then calculated in the same way for each algorithm, given the predicted events (see Supporting Materials and Methods).

Overall, FEATHER did an excellent job, essentially matching the performance of human-annotated data. In comparison to the best performance of either reference algorithm, FEATHER's prediction yielded rupture force and loading rate distributions which were eightfold closer to the human-annotated data and 30-fold better in an event location metric (ΔZ_{95}), as defined below. The top panel of Fig. 3 *A* shows that the distribution in the relative location error of the "true events," defined by an expert user, relative to predicted events ($d_{t\to p}$; *green shading*) closely matched the distance distribution from predicted events to true events ($d_{p\to t}$; *blue line*) (see Fig. 1 *F* for the definitions of $d_{t\to p}$ and $d_{p\to t}$ and the Supporting Materials and Methods for details of manual annotation). The peak of this distribution at low relative error shows precision in determining event location. The overlap between the two distributions shows that the number of true events closely matched the number of predicted events. However, such overlap was not present when the data were analyzed with OpenFovea, which showed a high number of false positives, as indicated by the gap between the distributions of $d_{p\to t}$ (*black line*) and $d_{t\to p}$ (*green shading*). We speculate that OpenFovea's performance may be limited in this application by a data set that contains both low- and high-force unfolding events, despite efforts to optimize OpenFovea's parameters for this data set (see Supporting Materials and Methods; Fig. S5). The wavelet-based scheme, which also had its parameters optimized for this data set, showed better performance on this metric than OpenFovea but still had a 30-fold higher relative location error and a threefold higher false-positive rate than FEATHER (Fig. S6). Relative to the better-performing wavelet scheme, FEATHER improved event localization precision ~30-fold based on ΔZ_{95} (Table 1), where ΔZ_{95} is defined as the location of the 95th percentile of the combined distribution for $d_{p\to t}$ and $d_{t\to p}$ (see Fig. 3 *A*; Table S5, *dashed line*). As defined, ΔZ_{95} represents a good metric for the upper bound of the error in determining event location.

Because an accurate determination of rupture force and loading rate is critical to deriving biological insight from force spectroscopy data (2,6,7), we next compared all three algorithms to human-annotated results for these two metrics (Fig. 3, *B* and *C*). As shown in the top panel of each column, FEATHER (*blue line*) essentially matched the human-annotated distributions (*green shading*), whereas OpenFovea showed a surplus of low-force unfolding events (*black line*) arising from its high false-positive rate. Again, the

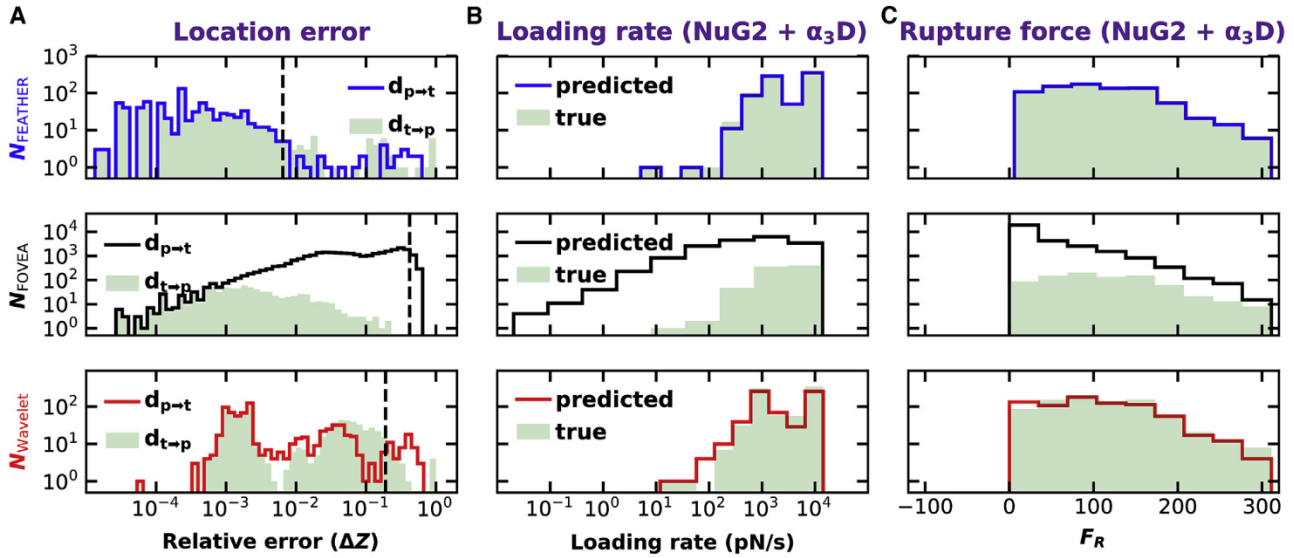

FIGURE 3 Evaluating FEATHER's performance. (*A*) Shown here are histograms of fractional errors between human-annotated and algorithmically predicted event locations for the polyprotein data set when using FEATHER, OpenFovea (12), and the wavelet-based scheme from Scientific Python (20), where ΔZ is the combined fractional distance between the identified and predicted events divided by the full range of the record, and the dotted line denotes the location of ΔZ_{95}, where ΔZ_{95} is defined as the location of the 95th percentile of the combined distribution for the fractional error $d_{p\to t}$ and $d_{t\to p}$. As diagrammed in Fig. 1 *F*, $d_{t\to p}$ is the distance from a human-annotated "true" event to the closest predicted event, and $d_{p\to t}$ is the distance from an algorithmically predicted event to the closest true event. (*B*) Shown here are histograms comparing the loading rates from manual-event annotation (*green*) to algorithmically predicted ones for FEATHER (*blue*), OpenFovea (*black*), and Scientific Python (*red*), respectively. Note, the green shaded distribution in all three panels represents the same data set but appears slightly different because of variations in bin size. (*C*) A histogram of rupture force for human-annotated and algorithmically determined events using the same color scheme is shown.

wavelet scheme showed intermediate performance (*red line*). Despite these distributions being oddly shaped because of the presence of both low-force (α_3D) and high-force (NuG2) ruptures over a range of v, we quantitatively compared the degree of overlap between the human-annotated and algorithmic results using Bhattacharya coefficient's complement (BCC; see Table S5) (21). By this metric, FEATHER outperforms the wavelet scheme by a factor of eight (Table 1). We note that in additional tests on a DNA data set purposely containing multiple tethers that led to multiple, closely spaced unfolding events at low force (10–30 pN), we saw even larger performance improvements of FEATHER by these metrics (Fig. S2 *E* and *F*; Figs. S7 and S8). In addition, FEATHER successfully analyzed hundreds of simulated ruptures over a wide range of contour length changes, loading rates, and rupture forces (Fig. S9; Table S6). Taken together, FEATHER's performance on experimental polyprotein data, an experimental DNA data set, and a complex simulated data set underscored the consistent strength of FEATHER's predictive power.

TABLE 1 The Performance Metrics for Each Algorithm

Name	BCC (↓)	ΔZ_{95} (↓)
FEATHER	0.0037	0.0065
OpenFovea	0.203	0.42
Scientific Python	0.030	0.19

BCC compares the degree of overlap between the human-annotated and algorithmically predicted two-dimensional distribution of rupture force versus loading rate (e.g., Fig. S7 *B*; Table S5). ΔZ_{95} is the metric for the upper bound of the fractional error in determining event location. The symbol (↓) indicates a lower value is better.

Conclusions

The canonical SMFS assay retracts a force probe at constant velocity to yield records containing unfolding and unbinding events. Here, we introduce FEATHER, which automatically determines event locations for such records and thereby determines the rupture force and loading rate. FEATHER requires only two simple-to-understand parameters to accurately and algorithmically recapitulate human-annotated data. Its fast execution and linear runtime with the number of data points allows for automated analysis of large data sets that, in turn, will allow for more sophisticated analysis that yields additional biophysical information, such as $\Delta G^{\ddagger}$ (7). When analyzing a complex data set containing both low- and high-force rupture events, FEATHER provided more than an order of magnitude improvement in event localization error (ΔZ_{95}) relative to other representative algorithms (Table 1) and did not bias the data toward high-force events. We note that the data sets used here were acquired with a relatively long, soft cantilever. Recent efforts in improving the precision and time resolution of AFM cantilevers will immediately aid FEATHER's ability to detect smaller and more closely spaced unfolding intermediates (22,23). By predicting

where events occur without relying upon any a priori domain-specific model of the event, FEATHER provides a powerful tool within a longer SMFS analysis pipeline (12,16). For instance, it can be used to segment complex force spectra to then determine the change in contour length between ruptures, a value which in turn can be used to screen large data sets for the unfolding of particular structures. Finally, we anticipate that FEATHER's underlying event detection algorithm can be extended to search for both unfolding and refolding events, increasing its utility to a broader array of force spectroscopy assays.

SUPPORTING MATERIAL

Supporting Materials and Methods, ten figures, eight tables, and four data files are available at http://www.biophysj.org/biophysj/supplemental/S0006-3495(18)30918-4.

AUTHOR CONTRIBUTIONS

P.R.H. conceived of and developed the algorithm. P.R.H. and T.T.P. designed the research. P.R.H. acquired the data. P.R.H. and T.T.P. analyzed the data and wrote the manuscript.

ACKNOWLEDGMENTS

We thank J. Boyd-Graber and R. Frongillo for discussions on algorithm development and M. A. LeBlanc for sharing the polyprotein data set. All of the analyzed force-extension curves, along with their annotation, are available from the Dryad Digital Repository (https://doi.org/10.5061/dryad.1615c2p).

This work was supported by the National Science Foundation (MCB-1716033 and Phy-1734006) and National Institute of Standards and Technology. T.T.P. is a staff member of the National Institute of Standards and Technology's Quantum Physics Division.

SUPPORTING CITATIONS

References (24–32) appear in the Supporting Material.

REFERENCES

1. Moy, V. T., E. L. Florin, and H. E. Gaub. 1994. Intermolecular forces and energies between ligands and receptors. *Science.* 266:257–259.
2. Merkel, R., P. Nassoy, …, E. Evans. 1999. Energy landscapes of receptor-ligand bonds explored with dynamic force spectroscopy. *Nature.* 397:50–53.
3. Rief, M., M. Gautel, …, H. E. Gaub. 1997. Reversible unfolding of individual titin immunoglobulin domains by AFM. *Science.* 276:1109–1112.
4. Kellermayer, M. S., S. B. Smith, …, C. Bustamante. 1997. Folding-unfolding transitions in single titin molecules characterized with laser tweezers. *Science.* 276:1112–1116.
5. Evans, E., and K. Ritchie. 1997. Dynamic strength of molecular adhesion bonds. *Biophys. J.* 72:1541–1555.
6. Evans, E., and K. Ritchie. 1999. Strength of a weak bond connecting flexible polymer chains. *Biophys. J.* 76:2439–2447.
7. Dudko, O. K., G. Hummer, and A. Szabo. 2006. Intrinsic rates and activation free energies from single-molecule pulling experiments. *Phys. Rev. Lett.* 96:108101.
8. Walder, R., M. A. LeBlanc, …, T. T. Perkins. 2017. Rapid characterization of a mechanically labile α-helical protein enabled by efficient site-specific bioconjugation. *J. Am. Chem. Soc.* 139:9867–9875.
9. Bosshart, P. D., P. L. Frederix, and A. Engel. 2012. Reference-free alignment and sorting of single-molecule force spectroscopy data. *Biophys. J.* 102:2202–2211.
10. Kuhn, M., H. Janovjak, …, D. J. Müller. 2005. Automated alignment and pattern recognition of single-molecule force spectroscopy data. *J. Microsc.* 218:125–132.
11. Gergely, C., B. Senger, …, J. Hemmerlé. 2001. Semi-automatized processing of AFM force-spectroscopy data. *Ultramicroscopy.* 87:67–78.
12. Roduit, C., B. Saha, …, S. Kasas. 2012. OpenFovea: open-source AFM data processing software. *Nat. Methods.* 9:774–775.
13. Kasas, S., B. M. Riederer, …, G. Dietler. 2000. Fuzzy logic algorithm to extract specific interaction forces from atomic force microscopy data. *Rev. Sci. Instrum.* 71:2082–2086.
14. García-Massó, X., M. C. Huber, …, J. L. Toca-Herrera. 2016. Automated detection of protein unfolding events in atomic force microscopy force curves. *Microsc. Res. Tech.* 79:1105–1111.
15. Benítez, R., and V. J. Bolós. 2017. Searching events in AFM force-extension curves: a wavelet approach. *Microsc. Res. Tech.* 80:153–159.
16. Galvanetto, N., A. Perissinotto, …, V. Torre. 2018. Fodis: software for protein unfolding analysis. *Biophys. J.* 114:1264–1266.
17. Partola, K. R., and G. Lykotrafitis. 2016. FRAME (force review automation environment): MATLAB-based AFM data processor. *J. Biomech.* 49:1221–1224.
18. Cao, Y., R. Kuske, and H. Li. 2008. Direct observation of markovian behavior of the mechanical unfolding of individual proteins. *Biophys. J.* 95:782–788.
19. Pittman, J. 1993. Probablility. Springer, New York.
20. Jones, E., E. Oliephant…, 2001. SciPy: Open source scientific tools for Python. *http://www.scipy.org/.*
21. Bhattacharyya, A. 1943. On a measure of divergence between two statistical populations defined by their probability distributions. *Bull. Calcutta Math. Soc.* 35:99–109.
22. Edwards, D. T., J. K. Faulk, …, T. T. Perkins. 2017. Force spectroscopy with 9-μs resolution and sub-pN stability by tailoring AFM cantilever geometry. *Biophys. J.* 113:2595–2600.
23. Bull, M. S., R. M. Sullan, …, T. T. Perkins. 2014. Improved single molecule force spectroscopy using micromachined cantilevers. *ACS Nano.* 8:4984–4995.
24. Marko, J. F., and E. D. Siggia. 1995. Stretching DNA. *Macromol.* 28:8759–8770.
25. Dierckx, P. 1975. An algorithm for smoothing, differentiation and integration of experimental data using spline functions. *J. Comput. Appl. Math.* 1:165–184.
26. Mohri, M., A. Rostamizadeh, and A. Talwalkar. 2012. Foundation of Machine Learning. MIT Press, Cambridge, MA.
27. Churnside, A. B., R. M. Sullan, …, T. T. Perkins. 2012. Routine and timely sub-picoNewton force stability and precision for biological applications of atomic force microscopy. *Nano Lett.* 12:3557–3561.
28. Proksch, R., T. E. Schaffer, …, M. B. Viani. 2004. Finite optical spot size and position corrections in thermal spring constant calibration. *Nanotechnology.* 15:1344–1350.
29. Bryson, J. W., J. R. Desjarlais, …, W. F. DeGrado. 1998. From coiled coils to small globular proteins: design of a native-like three-helix bundle. *Protein Sci.* 7:1404–1414.
30. Nauli, S., B. Kuhlman, and D. Baker. 2001. Computer-based redesign of a protein folding pathway. *Nat. Struct. Biol.* 8:602–605.
31. Hummer, G., and A. Szabo. 2010. Free energy profiles from single-molecule pulling experiments. *Proc. Natl. Acad. Sci. USA.* 107:21441–21446.
32. Wang, M. D., H. Yin, …, S. M. Block. 1997. Stretching DNA with optical tweezers. *Biophys. J.* 72:1335–1346.